Insect Biochemistry and Molecular Biology 109 (2019) 52–62

Contents lists available at ScienceDirect

Insect Biochemistry and Molecular Biology

journal homepage: www.elsevier.com/locate/ibmb

Molecular nature of dominant naked pupa mutation reveals novel insights into silk production in *Bombyx mori*

Wenbo Hu[a,b], Wei Lu[a,b], Liwan Wei[b], Yan Zhang[a,b], Qingyou Xia[a,b,*]

[a] Biological Science Research Center, Southwest University, Chongqing, 400716, PR China
[b] Chongqing Key Laboratory of Sericulture Science, Chongqing Engineering and Technology Research Center for Novel Silk Materials, Beibei, Chongqing, 400716, PR China

ARTICLE INFO

Keywords:
Bombyx mori
Silk secretion
Fibroin heavy chain
Gland atrophy
Naked pupa

ABSTRACT

Silks are natural protein biopolymers with desirable mechanical properties and play crucial roles in insect survival and reproduction. However, the mechanisms by which large amounts of silk fibroin are efficiently secreted from the protein production organs (silk glands) remain elusive. Here, we focus on a dominant silkworm mutation, naked pupa (*Nd*), which enables carriers to lose spinning behaviors, produce a deficiency of silk fibroin production, and result in degenerate posterior silk gland (PSG). Linkage mapping and sequencing analyses revealed a deletion of 19 bp of the *fibroin heavy chain* (*FibH*), which results in a frameshift-caused deletion of the C-terminal domain (CT) responsible for the *Nd* locus. Immunofluorescence and immunoblot analysis showed that the PSG cells with truncated FibH exhibit blockades in the secretion of all three fibroins (FibH, FibL, and P25) from silk gland cell to silk gland lumen (a secretion-deficiency). By comparing the hereditary characters of three naked silkworm mutations (*Nd*, *Nd-s*, and *fibH-ko*), we explored the relationship between dominant and recessive inheritances in naked silkworms and found that high-molecular-weight/repetitive FibH with secretion-deficiency was in positive correlation with PSG atrophy phenotype, and moreover, the repetitive region of *Nd*-FibH accounted for the dominant phenotypes of fibroin secretion-deficiency, PSG atrophy, and naked pupa in *B. mori*. Our results uncovered the molecular nature of the silkworm *Nd* mutation and significantly improved our understanding of fibroin synthesis and secretion in silk-spinning caterpillars.

1. Introduction

Animal silks are outstanding natural materials spun by several arthropod lineages that have existed for hundreds of millions of years (Liu and Zhang, 2014). Genetic and evolutionary studies show that over 850,000 insect species in 16 orders produce different types of silk for a wide variety of purposes (Babb et al., 2017; Craig, 1997; Sanggaard et al., 2014). In nature, insect silks are primarily used as building materials to construct cocoons (Lepidoptera and Trichoptera) (Yonemura and Sehnal, 2006; Yonemura et al., 2006), as well as build webs (Araneida) (Vollrath, 1999) and elaborate nests (Ephemeroptera and Embiodea) (Okada et al., 2008; Sattler, 1967); produce webs to cover parasitized hosts/eggs (Hymenoptera/Coleoptera, respectively) (Oberprieler et al., 2007; Sutherland et al., 2007); produce threads to capture prey (Trichoptera and Diptera) (Rudall, 1962; Yonemura et al., 2006); or as stalks to transfer sperm (Archaeognatha) (Sturm, 1992). The remarkable mechanical properties of silk have attracted the interest of biologists, chemists, and material scientists for over a century (Altman et al., 2003; Fu et al., 2009).

To date, the most well-studied insect silks are those produced by caterpillars of the lepidopteran *Bombyx mori* (Omenetto and Kaplan, 2010; Shao and Vollrath, 2002). Native silk from *B. mori* cocoons is composed of silk fibroin protein together with a family of sericin proteins to glue the fibroin brins together to form the cocoon (Andersson et al., 2016; Xia et al., 2014). The sericins are adhesive proteins that account for 25–30% of the total *B. mori* cocoon by weight. The silk fibroins are a 2300 kDa molecular complex, consisting of six sets of disulfide-linked fibroin heavy (FibH, 350 kDa) and light (FibL, 25 kDa) chains and a fibrohexamerin protein (P25, 30 kDa) at a molar ratio of 6:6:1 (Aramwit et al., 2012; Inoue et al., 2000). Additionally, the twentieth cysteine residue from the C-terminal domain (CT) of FibH (Cys-c20) is important for the formation of disulfide linkage with FibL,

Abbreviations: Nd, naked pupa; L5D3, the 3rd day of the fifth larval instar; ASG, anterior silk gland; MSG, middle silk gland; PSG, posterior silk gland; BC1, backcrossed F1; SNP, single nucleotide polymorphism; FibH, fibroin heavy chain; FibL, fibroin light chain; NT, N terminal domain; CT, C terminal domain; R, repetitive domain; A, amorphous domains; FITC, fluorescein isothiocyanate; DAPI, 4′,6-diamidino-2-phenylindole

* Corresponding author. Biological Science Research Center, Southwest University, Chongqing, 400716, PR China.
E-mail address: xiaqy@swu.edu.cn (Q. Xia).

https://doi.org/10.1016/j.ibmb.2019.04.006
Received 20 February 2019; Received in revised form 1 April 2019; Accepted 1 April 2019
Available online 04 April 2019
0965-1748/

which is essential for the secretion of fibroin from the silk gland cells into the lumen (Tanaka et al., 1999b).

In the silk-producing organ (silk gland), large amounts of high-molecular-weight fibroin complex are secreted efficiently and stored at high concentrations without aggregation or denaturalization (Askarieh et al., 2010; Hu et al., 2016). Elucidation of the molecular mechanisms underlying protein processing in silk glands is crucial for recapturing the natural properties *in vitro* in reconstituted or genetically engineered silks (Jin and Kaplan, 2003). However, these detailed molecular mechanisms are still unknown. Because of the advantages in artificial breeding and large silk protein production, and further, the silk filament in most lepidopteran families is formed from a complex of FibH, FibL, and P25 (Fedic et al., 2002), the *B. mori* represents an excellent model organism for understanding the process of silk protein synthesis and secretion in lepidopteran caterpillars.

Numerous *B. mori* mutants with diverse cocoon colors, shapes, and qualities serve as useful resources for studying multiple aspects of silk formation. Among these, the most useful for researchers are fibroin-deficient (cocoon quality) mutants that are valuable tools for studying the process of fibroin synthesis and secretion in the silk gland (Goldsmith et al., 2005). Molecular genetic studies have revealed the importance of the FibH-FibL subunit combination for the efficient secretion of fibroin from the posterior silk gland (PSG) cells using the *Nd-s/Nd-s*^{D} (*FibL* mutation) and *Nd(2)* (unresolved mutation) mutants (Mori et al., 1995; Takei et al., 1987). The *FibH* knock-out (*fibH-ko*) mutant, which was generated by genome editing, has different phenotypes according to the indels occurring at different *FibH* gene target sites. The mutant *FibH* encoding mutant FibH with 118 aa (only NT) produce a normal silk gland with highly efficient synthesis and secretion of the exogenous protein (Ma et al., 2014), and with 286 aa (NT and partial repetitive region) produce poorly developed silk gland (Cui et al., 2018; Wang and Nakagaki, 2014).

The first *B. mori* fibroin-deficient mutant was identified in 1933 and known as a *Naked pupa* (*Nd*, a dominant mutation) (Nakano, 1951). Since then, the *Nd* locus (0.0 cM) has become a ubiquitous twenty-fifth chromosomal marker used by *Bombyx* geneticists to track mutations. Despite its widespread use, the *Nd* mutant gene and underlying mutational mechanism remain unknown. In this study, we reveal the molecular nature of the dominant *Nd* mutation: a deletion of 19 bp in A07 of *FibH* leads to premature translational termination and results in a CT-deleted FibH. Further, we show that the CT-deleted FibH causes fibroin secretion-deficiency and PSG atrophy. The results suggest that the intact and conserved CT of FibH contributes to fibroin secretion from PSG cells to the lumen; this process, which may be conserved among Lepidoptera, ensures the successful secretion of the high-molecular-weight fibroin complex.

2. Material and methods

2.1. Silkworm strains

Mutant strains for *Naked pupa* (*Nd*), *Nd-s* mutant (Inoue et al., 2005; Mori et al., 1995) and *FibH* knock-out (*fibH-ko*) (Ma et al., 2014), and wild-type strain Dazao (WT/Dazao) were obtained from the Silkworm Gene Bank and the Silk Science and Technology Research Group, Southwest University (Chongqing, China). *Nd* mutants, *Nd-s* mutants, and *fibH-ko* mutants were crossed with WT/Dazao to obtain their F1 progeny. Silkworms were reared on fresh mulberry leaves at a constant temperature of 25 °C on a 12: 12 h light: dark cycle.

2.2. Positional cloning of the Nd locus

For positional cloning of the *Nd* locus, nine F1 heterozygous males were obtained from a single-pair cross between an *Nd* mutant female and WT/Dazao male, and each was backcrossed with a WT/Dazao female (BC1 generation). A total of 1317 BC1 pupae were used for analysis. Genomic DNA was extracted from parent moths, F1 moths, and each of the BC1 pupae using DNAzol reagent (Invitrogen, USA), and purified using PI-1200 (Kurabo, Japan). To construct the *Nd* linkage map, SNP markers on chromosome 25 and newly developed markers from the silkworm genome sequence (Wang et al., 2005; Xia et al., 2004) were used to survey the segregation patterns in the 1317 BC1 individuals. Primers for the SNP markers used in the linkage map analysis are listed in Table S1.

2.3. Total RNA extraction and qRT-PCR

Total silk gland (MSG and PSG) RNA was extracted from the *Nd* mutant, *Nd-s* mutant, *fibH-ko* mutant, and WT/Dazao using TRIzol reagent (Invitrogen, USA). Reverse transcription was performed on total RNA (1 mg) using a random primer (N6), an oligo (dT) primer, and the PrimeScript RT reagent Kit using gDNA Eraser (Takara, Japan) according to the manufacturer's protocols. The qRT-PCR was performed using a qTOWER 2.0 real-time PCR system (Analytik Jena, Germany) and SYBR *Premix Ex Taq* II (Takara, Japan) according to the manufacturer's protocols. The silkworm housekeeping gene *ribosomal protein L3* (*Rpl3*: GenBank accession number NM_001043661.1) was used as the internal control for RNA normalization. Primer sets for qRT-PCR are listed in Table S1. Three independent replicates were analyzed.

2.4. PacBio sequencing

For single-molecule real-time (SMRT) sequencing, the PacBio sequencing primer was annealed to the eluted SMRTbell template (Pacific Biosciences, USA) and purified with 0.6× AMPure beads (Pacific Biosciences, USA) to remove unbound primers. A modified polymerase binding protocol with free hairpin adapters in the binding buffer was used to bind excess DNA polymerase. Sequencing data were collected on a PacBio RSII instrument (Pacific Biosciences, USA) using the one-cell-per-well MagBead sequencing protocol, P6/C4 sequencing chemistry, and 6-h collection time.

2.5. Antigen design and antibody preparation

The amino acid sequence of silkworm FibH (GenBank accession number AF226688.1) was retrieved from the NCBI public database (Zhou et al., 2000). Residues “GGYSRSDGYEY,” “AWSSESDFGT,” and “SASSRSYDYSRRNV” were selected as antigens of amorphous domain 01 (A01), amorphous domain 02–10 (A02–10), and the CT, respectively. The peptide synthesis and antibodies preparation were performed by Zoonbio Biotechnology Co., Ltd (China). The polyclonal antibody against the N-terminal domain (NT, residues 20–126) of FibH was provided by Prof. Congzhao Zhou from University of Science and Technology of China.

2.6. Sections and immunostaining

Silk glands were fixed using 4% (v/v) paraformaldehyde/PBS, dehydrated in a gradient ethanol series from 70% to 100%, embedded in paraffin, and cut into 5-μm sections. After deparaffinizing, silk gland sections were incubated for 20 min at 95 °C and allowed to cool at room temperature in 0.01 M citric acid buffer solution (pH 6.0) for antigen retrieval, followed by blocking for 60 min at 37 °C in PBS containing 10% (v/v) normal goat serum. Subsequently, samples were treated with primary antibodies (1:100) for 60 min at 37 °C before incubation for 60 min at 37 °C with FITC-labeled secondary goat anti-rabbit IgG antibody (1:500, Beyotime, China). Finally, the samples were mounted using a mounting medium containing 4′,6-diamidino-2-phenylindole (DAPI).

2.7. Immunoblot analysis

Protein samples were prepared using a modified version of a previously reported method (Teramoto and Kojima, 2014). Briefly, silk glands/cocoon shells (10 mg per sample) were dissolved in 500 μL of 9 M LiSCN, diluted 10-fold in 8 M urea solution, mixed with a half-volume of 3 × SDS-PAGE sample buffer, and incubated for 30 min at room temperature. The protein concentration was then measured using the Bradford protein assay (Beyotime, China). Protein samples (20 μg) were separated using NuPAGE 4–12% Bis-Tris protein gel (Thermo Fisher Scientific, USA) and detected using Coomassie Brilliant Blue staining and by immunoblotting using HRP-conjugated FibH/FibL/P25-specific antibody (Ma et al., 2014).

2.8. Dissolving capacity analysis

Cocoon shells (20 mg per sample) were cut into small pieces, dissolved in 1 ml 8 M urea solution, and incubated for 30 min at 85 °C. Subsequently, samples were washed by pure water. Finally, the samples were dried for 120 min at 60 °C and weighed.

2.9. Statistical analysis

Statistical differences were evaluated using Student's *t*-test for unpaired samples. The level of statistically significant difference was set at * P value $<$ 0.05, ** P value $<$ 0.01, and *** P value $<$ 0.001.

3. Results

3.1. Silk secretion-deficiency affects spinning behaviors of B. mori

Silk threads play crucial roles in the survival of insects (Sutherland et al., 2010). To simulate stress conditions experienced by neonatal silkworm larvae, we turned egg papers upside-down and tapped them continuously. Normal silkworms (WT/Dazao) were hung in the air by their silks. Silkworms carrying the *Nd* mutation (*Nd* mutants) fell to the ground and were unable to spin silk of normal mechanical strength (Fig. 1A). At the molt stage, WT/Dazao spun small amounts of silk to anchor their bodies to the substratum; however, *Nd* mutants were unable to spin silk (Fig. 1B). At the mounting stage, *Nd* mutants only spun a thin and easily broken cocoon that consisted mostly of silk sericin (Fig. 1C); this cocoon was unable to protect the pupa effectively during metamorphosis. Anatomical observations of the silk gland at the 3rd day of the fifth larval instar (L5D3) showed that the PSG of the *Nd* mutant (*Nd*-PSG) was extremely short and degenerate, while that of WT/Dazao (WT-PSG) was long and folded (Fig. 1D). These findings imply that silk fibroin secretion and silk gland development in *Nd*-PSG are deficient.

3.2. Linkage analyses of B. mori Nd locus

The *Nd* was a dominant mutation and a qualitative trait. The phenotypic character of F1 individuals was naked pupa. To identify the gene responsible for the *Nd* phenotype, we conducted low-resolution mapping for 96 back-crossed F1 (BC1; Fig. S1) individuals using eight standard single nucleotide polymorphism (SNP) markers (Yamamoto et al., 2008) (Fig. 2A and Table S1), followed by fine mapping for 1221 BC1 individuals using newly designed SNP markers (Fig. 2B and Table S1). We found that five SNP markers (SNP34, SNP35, SNP39, SNP40, and SNP42 in Fig. S2) were completely linked to each phenotype in all BC1, which indicated that the narrowed 573 kb genomic region between markers "SNP25" and "SNP33" on chromosome 25 contained the gene responsible for the *Nd* phenotype (Fig. 2C). This region included 13 predicted genes (*BGIBMGA005078*, *BGIBMGA005079*, *BGIBMGA005080*, *BGIBMGA005081*, *BGIBMGA005082*, *BGIBMGA005111*, *BGIBMGA005112*, *BGIBMGA005113*, *BGIBMGA005114*, *BGIBMGA005115*, *BGIBMGA005116*, *BGIBMGA005117*, and *BGIBMGA005118*), and the ID of these genes is abbreviated as a number (e.g., *5111*: *BGIBMGA005111*).

3.3. Identification of the mutant FibH as the defective gene in the Nd locus

As the PSG was degenerate but the MSG was normal in *Nd* mutants (Fig. 1D), the gene responsible for the *Nd* phenotype was expected to be only differentially expressed in the *Nd*-PSG. We further analyzed the expression profiles of the 13 initial candidate genes in silk glands (PSG and MSG) at the L5D3 using RT-PCR (Fig. 3A and Fig. S3). Among these genes, only *BGIBMGA005111* had the predicted characteristics and was down-regulated in the *Nd*-PSG. Amplifications using different PCR cycles (20, 25, and 30) and qRT-PCR showed a consistent expression profile (Fig. 3B and C). Furthermore, *BGIBMGA005111* encodes partial fragment (Fig. 2C) of fibroin heavy chain (FibH), the core of silk fibroin, a low expression level of *FibH* might be responsible for the thin cocoon.

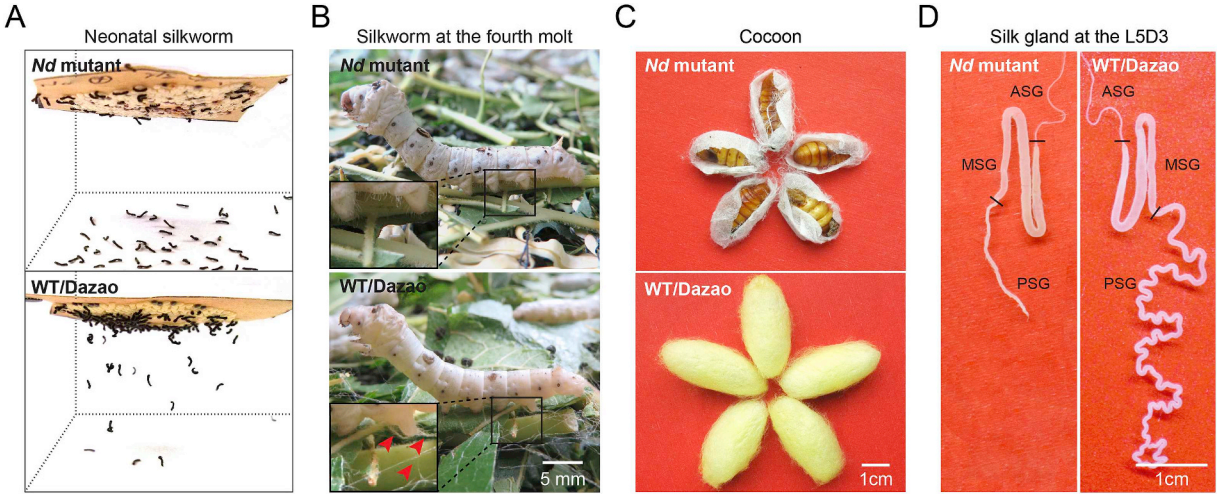

Fig. 1. Larval spinning behaviors of the *B. mori Nd* mutant. (A) Silk spinning behavior of neonatal *Nd* mutants and WT/Dazao under stress conditions when they were tapping on upside-down egg papers. (B) Silk spinning behavior of *Nd* mutants and WT/Dazao at the molt stage. The black box indicates the abdomen feet of the silkworm, and red arrowheads point to the silks under abdomen feet. (C) Cocoon shape of *Nd* mutants and WT/Dazao. (D) Silk gland of *Nd* mutants and WT/Dazao at the 3rd day of the fifth instar (L5D3). ASG, anterior silk gland; MSG, middle silk gland; PSG, posterior silk gland. (For interpretation of the references to color in this figure legend, the reader is referred to the Web version of this article.)

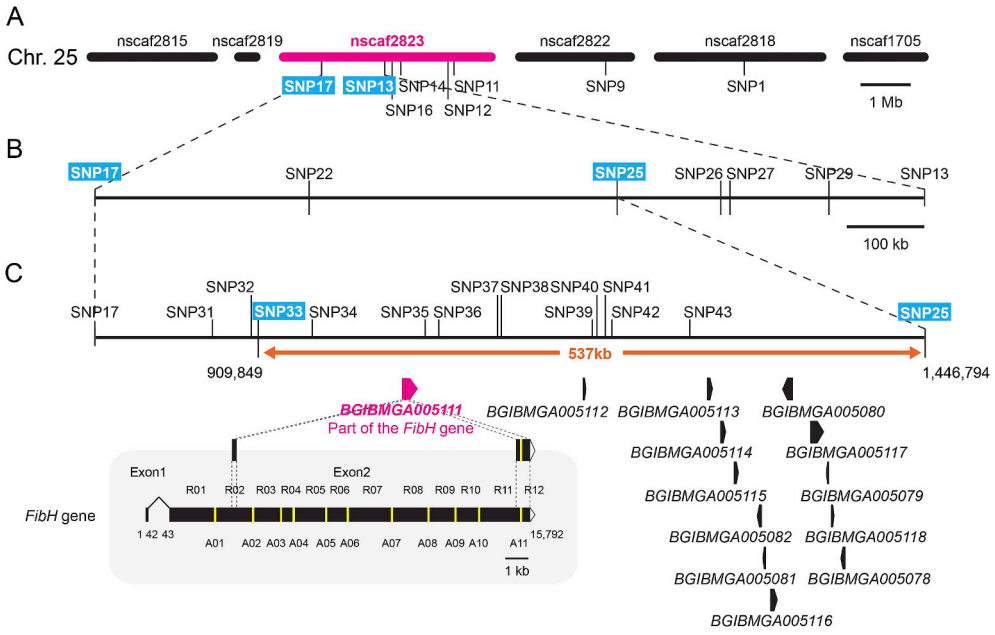

Fig. 2. Mapping of the *Nd* mutation on linkage group 25. (A) SNP markers used for approximate mapping to define the region linked to the *Nd* phenotype. The approximate region linked to the *Nd* phenotype was narrowed down with the blue markers, SNP13 and SNP17, using 96 BC1 individuals. (B) Newly developed SNP markers used for fine mapping to narrow the region tightly linked to the *Nd* phenotype using 1221 BC1 individuals. (C) Gene annotation in the *Nd* linked region. Thirteen genes were predicted in this region, including *BGIBMGA005078*, *BGIBMGA005079*, *BGIBMGA005080*, *BGIBMGA005081*, *BGIBMGA005082*, *BGIBMGA005111*, *BGIBMGA005112*, *BGIBMGA005113*, *BGIBMGA005114*, *BGIBMGA005115*, *BGIBMGA005116*, *BGIBMGA005117*, and *BGIBMGA005118*. The SNP markers with blue background narrow the candidate region in each round, and the 537 kb region responsible for the *Nd* phenotype is denoted by *Nd*:537-kb. SNP, single nucleotide polymorphism. (For interpretation of the references to color in this figure legend, the reader is referred to the Web version of this article.)

Taken together, we speculate that *FibH* is the gene responsible for the *Nd* mutation.

The *FibH* CDS encodes 5263 amino acid residues (350 kDa), containing 12 repetitive (R01-12) and 11 amorphous (A01-11) domains between the NT and CT (Zhou et al., 2000). To determine the mutation site, we cloned the *FibH* from *Nd* mutant (*Nd-FibH*) and sequenced it using the PacBio system. Coding sequences comparison and analysis showed that a deletion of 19 bp in A07 led to translational frameshifting and termination in R08 (Fig. 3D and Fig. S4), which resulted in a deletion of a partial repetitive domain and entire CT of FibH (Truncated FibH with theoretical Mw: 270 kDa) (Fig. 3E).

3.4. Protein level validation of the truncated FibH in Nd mutant

To further confirm the mutational pattern, we first successfully prepared four antibodies against FibH NT, A01, A02–10, and CT based on the intact FibH amino acid sequence of WT/Dazao (WT-FibH; AAF76983) (Fig. 4A). Then we performed subcellular localization of the FibH in *Nd*-PSG and WT-PSG. Immunofluorescence analysis of PSG sections revealed that the fluorescence signals (NT, A01, and A02-10)

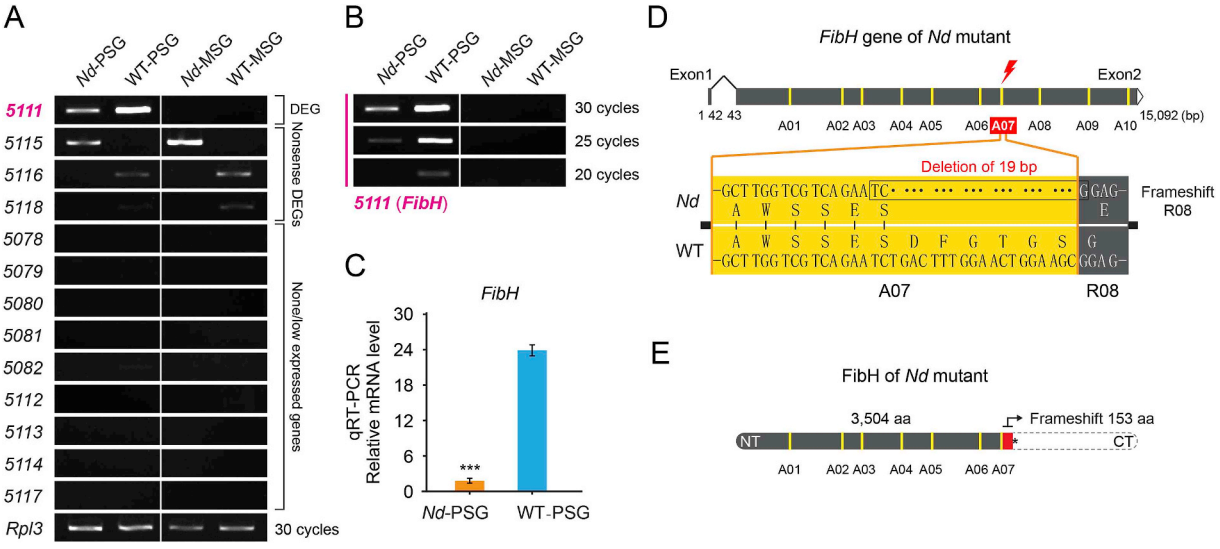

Fig. 3. Candidate genes analyses and schematic structure of the *Nd* mutant sites. (A) Expression profiles of thirteen candidate genes in the MSG and PSG of *Nd* mutants and WT/Dazao at the 3rd day of the fifth instar. The ID of candidate genes is abbreviated as a number (e.g., *5111*: *BGIBMGA005111*). MSG, middle silk gland; PSG, posterior silk gland; DEG, differentially expressed gene. (B) The expression level of *5111* (*FibH*) under different amplification cycles. *FibH*, *fibroin heavy chain* gene. (C) Quantitative RT-PCR analysis of *FibH* expression level in *Nd*-PSG and WT-PSG. Expression of the silkworm housekeeping gene *ribosomal protein L3* (*Rpl3*) was used as a control. Values are means ± SD (n = 3). Asterisks represent significant differences determined by a Student's *t*-test at *P* value < value (***). (D) Mutation site of the *Nd-FibH*. The yellow box indicates the amorphous region, and grey box indicates the repetitive region. R, the repetitive domain of *FibH*; A, the amorphous domain of *FibH*. (E) Schematic diagram of the *Nd*-FibH structure. NT, N-terminal domain; CT, C-terminal domain. (For interpretation of the references to color in this figure legend, the reader is referred to the Web version of this article.)

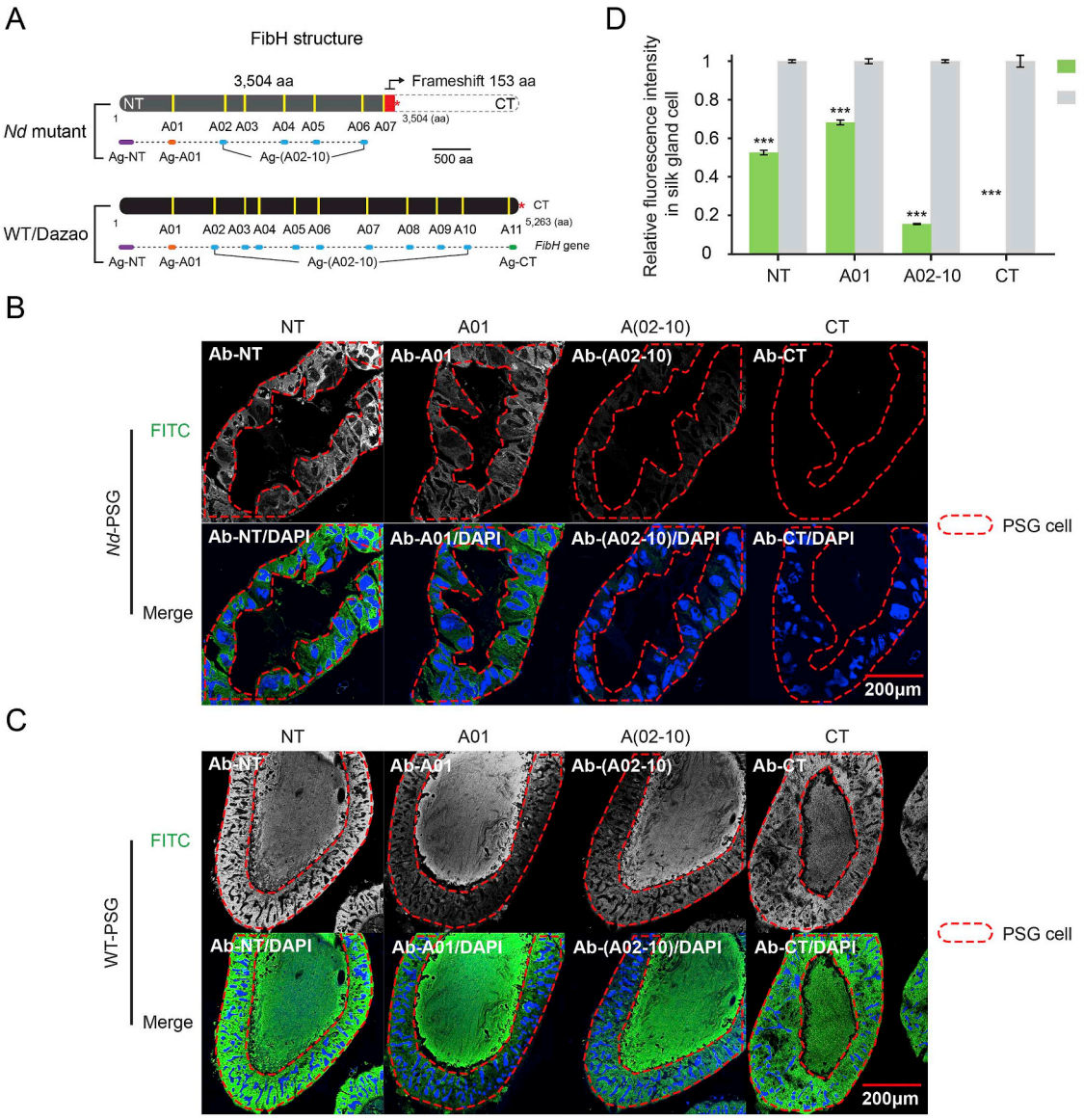

Fig. 4. Immunofluorescence localization of FibH in PSG. (A) Schematic diagram of the FibH protein structure and antigens location in FibH. NT, N-terminal domain; CT, C-terminal domain; A, amorphous domain; Ag, antigen. (B, C) FibH immunofluorescence with four antibodies in the *Nd*-PSG (B) and WT-PSG (C) cross-sections. FibH is shown in green and cell nucleus is shown in blue. Red dotted lines indicate the boundary of the PSG cell. Bull serum albumin was used to replace the primary antibody as a control. FITC, fluorescein isothiocyanate; Ab, antibody. (D) Relative fluorescence intensity of four FibH regions in PSG cell. Values are means ± SD (n = 3). Asterisks represent significant difference determined by Student's *t*-test at *P* value < 0.001 (***). (For interpretation of the references to color in this figure legend, the reader is referred to the Web version of this article.)

for *Nd*-FibH existed only in PSG cells, and not in the PSG lumen (Fig. 4B); however, the fluorescence signals (NT, A01, A02-10, and CT) for WT-FibH were emitted by both PSG cells and lumen (Fig. 4C). We additionally observed that the A02–10 fluorescence intensity was significantly decreased in *Nd*-PSG cells; moreover, no CT fluorescence signals were observed in *Nd* mutants (Fig. 4D). These results indicate that partial repetitive domain and entire CT of *Nd*-FibH was deleted, and the truncated FibH was blocked in PSG cell and not secreted to the lumen.

3.5. Truncated FibH induces loss-of-function of the PSG

The last larval instar (fifth instar) is the period during which the most vigorous silk protein synthesis and secretion occur in the silk gland of *B. mori*. To examine the processes of fibroin synthesis and transport in silk gland of the *Nd* mutant, SDS-PAGE and immunoblot analyses were performed at the 7th day of the fifth instar (L5D7). The SDS-PAGE analysis of total proteins in PSG showed an obvious FibH band (350 kDa) only in WT-PSG (Fig. 5A). Immunoblot analysis of FibH showed that, in the *Nd*-PSG, an immune band lower than the size of the 350 kDa WT-FibH band was detected by using the FibH-NT antibodies (Fig. 5B), which was consistent with the sequence analysis, suggesting that the lower band (240–350 kDa) represented *Nd*-FibH. Immunoblot analysis of FibL and P25 detected their respective immune bands both in the *Nd*-PSG and WT-PSG (Fig. 5C and D). Interestingly, the P25 in WT-PSG showed two immune bands, while that of *Nd*-PSG showed a single immune band with a molecular weight between the two bands (Fig. 5D).

The SDS-PAGE analysis of total proteins in MSG showed FibH and sericin bands in WT-MSG, but only sericin bands in *Nd*-MSG (Fig. 5E). Immunoblot analysis of three fibroin proteins (FibH, FibL, and P25) showed none of them was detected in *Nd*-MSG (Fig. 5F–H). These results suggested three fibroin proteins only in the *Nd*-PSG, but not in the *Nd*-MSG. Combined with immunofluorescence results in Fig. 4B, we

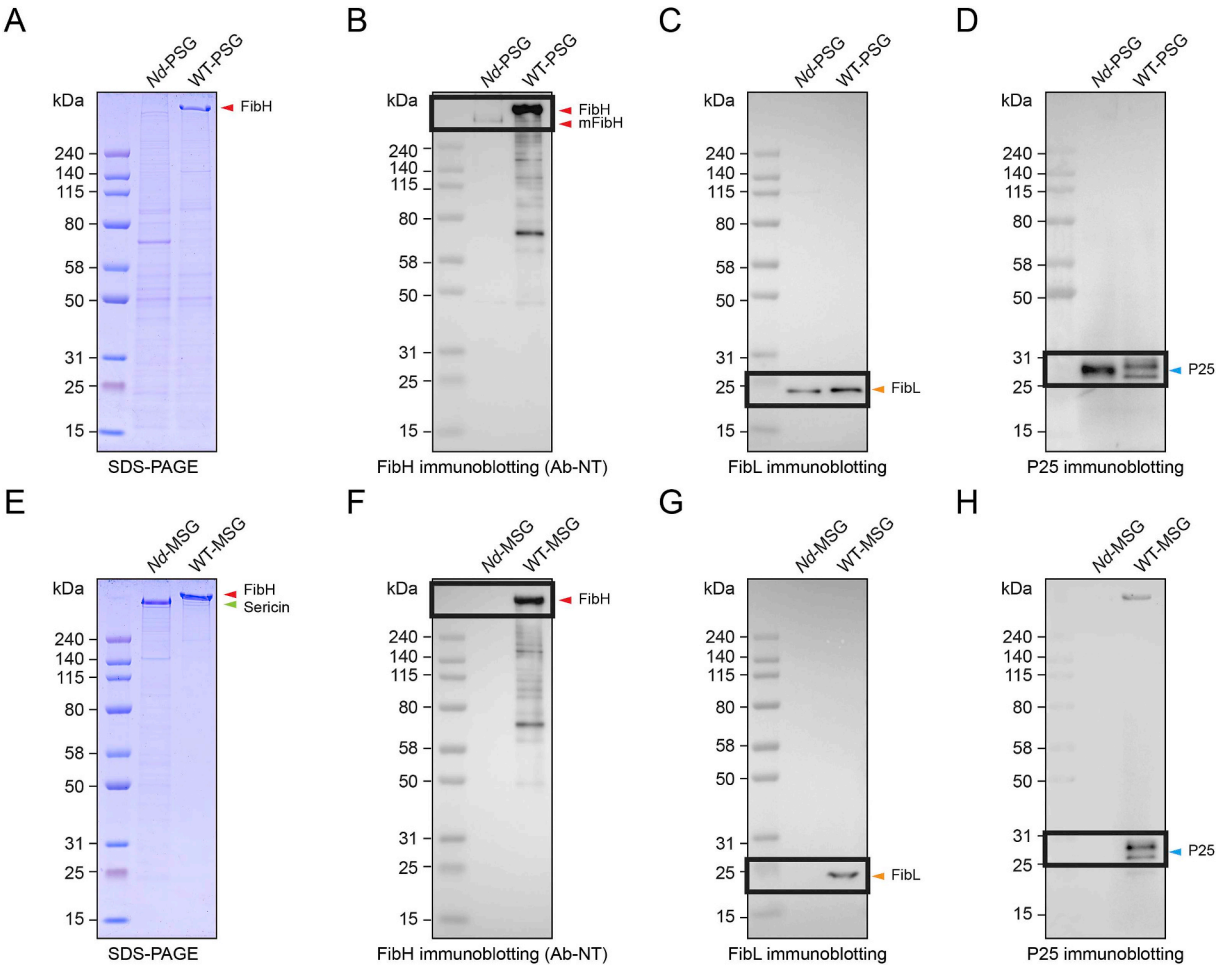

Fig. 5. Immunoblot analysis of three fibroin proteins in silk gland. (A) The SDS-PAGE analysis of total proteins in *Nd*-PSG and WT-PSG. The gel was stained by Coomassie brilliant blue. (B–D) Immunoblot analysis of FibH (B), FibL (C), and P25 (D) in *Nd*-PSG and WT-PSG. (E) The SDS-PAGE analysis of total proteins in *Nd*-MSG and WT-MSG. The gel was stained by Coomassie brilliant blue. (F–H) Immunoblot analysis of FibH (F), FibL (G), and P25 (H) in *Nd*-MSG and WT-MSG. The red arrowhead points to the FibH, the orange arrowhead points to the FibL, the blue arrow points to the P25, and the green arrowhead points to the sericin. (For interpretation of the references to color in this figure legend, the reader is referred to the Web version of this article.)

speculated that fibroin protein was not secreted from *Nd*-PSG cell to lumen or transported from *Nd*-PSG to *Nd*-MSG, and the basic protein secretory system of *Nd*-PSG was disrupted.

3.6. Genetic analysis of cocoon component in three naked pupa mutants

To further clarify the role of the truncated FibH in silk production defects, we compared the genetic characteristics of cocoon shape and component in three different fibroin-deficient mutants (*Nd* mutant (Truncated FibH), *Nd-s* mutant (Frameshift FibL) (Inoue et al., 2005; Mori et al., 1995), and *fibH-ko* mutant (NT-remaining FibH) (Ma et al., 2014)) and their hybrids with WT/Dazao. Firstly, we collected the cocoons produced by mutant strains, dissolved them in 8 M urea solution (Fig. 6A), and found that homozygous *Nd*-cocoon, *Nd-s*-cocoon, *fibH-ko*-cocoon, and heterozygous *Nd*/+-cocoon were all thin, fragile, and completely dissolved in 8 M urea solution (extracting sericin), but heterozygous *Nd-s*/+-cocoon and *fibH-ko*/+-cocoon became thicker and insoluble (Fig. 6B). Cocoon solubility measurements showed that the contents of an insoluble matter (mainly fibroin) in heterozygous *Nd-s*/+-cocoon and *fibH-ko*/+-cocoon reached half of WT-cocoon and WT-cocoon level respectively (Fig. 6C).

Then SDS-PAGE analysis of total proteins in homozygous cocoon showed FibH and sericin bands in WT-cocoon, but only sericin bands in *Nd*-cocoon, *Nd-s*-cocoon, and *fibH-ko*-cocoon (Fig. 7A). Immunoblot analysis of three fibroin proteins (FibH (Ab-NT), FibL, and P25) showed none of them was detected in *Nd*-cocoon and *Nd-s*-cocoon (Fig. 7B–D), and moreover, FibL and P25 were detected in *fibH-ko*-cocoon. Interestingly, the P25 in WT-cocoon showed two immune bands, while that of *fibH-ko*-cocoon showed a single immune band with a molecular weight between the two bands (Fig. 7D), which was consistent with the result in Fig. 3D. The SDS-PAGE analysis of total proteins in heterozygous cocoon showed FibH and sericin bands in *Nd-s*/+-cocoon and *fibH-ko*/+-cocoon, but still only sericin bands in *Nd*/+-cocoon (Fig. 7E). Immunoblot analysis of three fibroin proteins (FibH, FibL, and P25) showed they were detected in *Nd-s*/+-cocoon and *fibH-ko*/+-cocoon, but none of them was detected in *Nd*/+-cocoon (Fig. 7F–H). These results suggested that the truncated FibH induced a dominant mutant phenotype in silkworm carrying *Nd* mutation, and in *Nd*/+ mutant, the fibroin unit (FibH-FibL-P25 complex with a 6:6:1 molar ratio) was secretion-deficient when truncated FibH was added.

3.7. The repetitive region of Nd-FibH accounts for secretion-deficiency and PSG atrophy

In addition, based on the fact that PSG is responsible for synthesis and secretion of three fibroins, the criterion for evaluating the functional integrity of the secretory system is whether it secretes fibroin or not. Therefore, the results of genetic analysis of cocoon component suggested a normal system of protein secretion (at least one of the fibroin was secreted) in the *fibH-ko*-PSG, WT-PSG, *Nd-s*/+—PSG, and

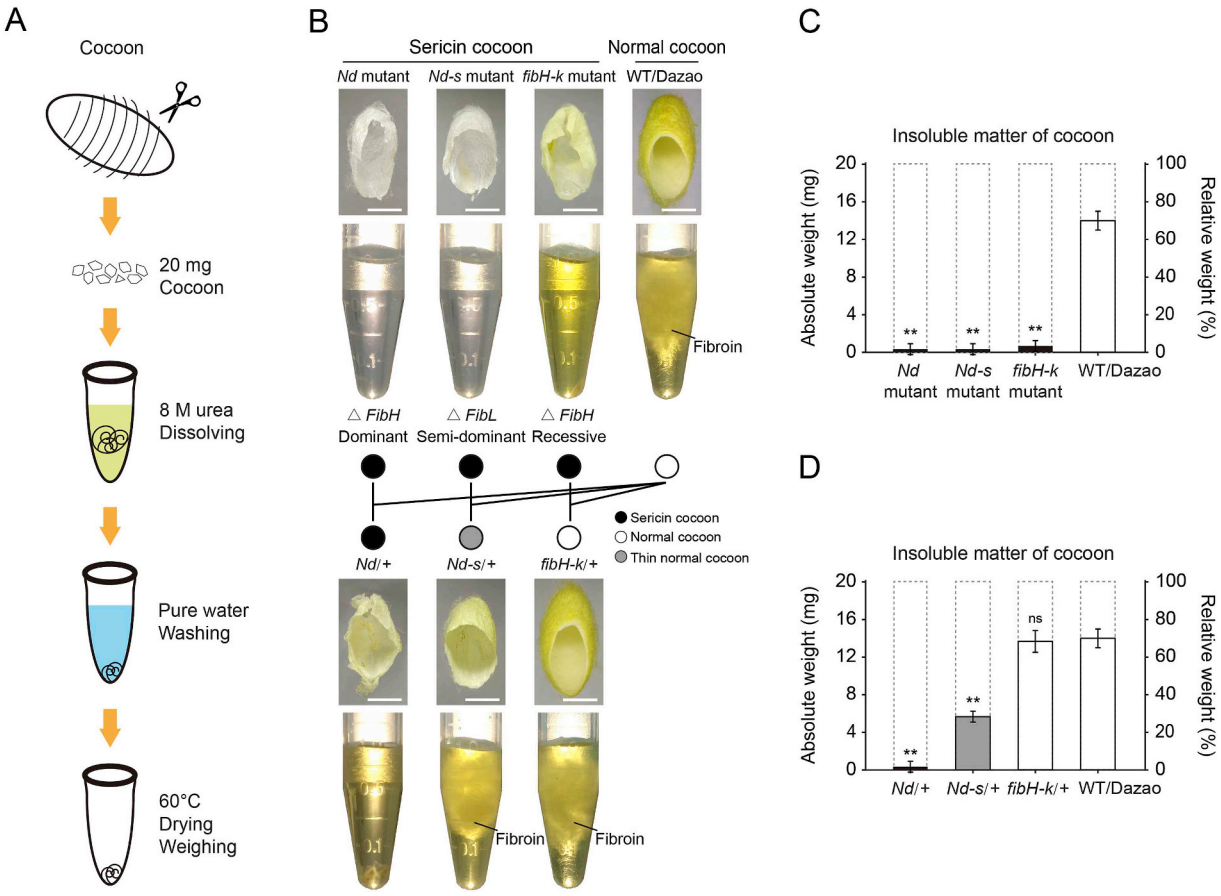

Fig. 6. Cocoon phenotype analysis of three different fibroin-deficient mutants. (A) Experimental flow for dissolving capacity analysis of cocoon silk. (B) Cocoon phenotypes of homozygous mutants (*Nd* mutant, *Nd-s* mutant, and *fibH-k* mutant) and heterozygous mutants (*Nd/+* mutant, *Nd-s/+* mutant, and *fibH-k/+* mutant). Cocoons are dissolved in 8 M urea solution. (C–D) Insoluble matter in the cocoon of homozygous mutants (C), heterozygous mutants (D). Values are means ± SD (n = 3). Asterisks represent significant difference determined by Student's *t*-test at *P* value < 0.01 (**), *P* value < 0.001 (***).

fibH-ko/+−PSG, but a deficient system of protein secretion (none of the fibroin was secreted) in the *Nd*-PSG, *Nd-s*-PSG, and *Nd/+*−PSG (Fig. 8A). To explore the relationship between the secretion-deficiency and PSG developmental defect, we investigated the morphology of the silk glands in three different fibroin-deficient mutants and their hybrids with WT/Dazao. As shown in Fig. 8B, the WT-PSG, *fibH-ko*-PSG, *Nd-s/+*−PSG, *fibH-ko/+*−PSG, with a normal system of protein secretion, were long and folded, but the *Nd*-PSG, *Nd-s*-PSG, and *Nd/+*−PSG, with a deficient system of protein secretion, were short and degenerate. These results revealed a positive correlation between secretion-deficiency and PSG atrophy.

Among the *Nd* mutant, *fibH-ko* mutant, and WT/Dazao, the WT-FibH (intact FibH) contains three substructures (NT, repetitive region, and CT), the *Nd*-FibH (Truncated FibH) contains NT and repetitive region, and the *fibH-ko*-FibH only contains NT (Ma et al., 2014). The protein structural difference between *Nd*-FibH (Not secreted) and WT-FibH (Secreted) is a CT (Fig. 8C), and that between *Nd*-FibH (Not secreted) and *fibH-ko*-FibH (Secreted) is a repetitive Gly-Ala-rich region (Fig. 8D). Combining the above results, we concluded that the CT might contribute to the efficient secretion of FibH, and the repetitive region might account for secretion-deficiency of the *Nd*-FibH.

4. Discussion

B. mori fibroin-deficient mutants have been widely used as genetic resources to study the silk production process; however, the molecular nature underlying the *Nd* mutation has remained obscure for over 80 years. In this study, we constructed a high-density linkage map of *Nd* locus on chromosome 25th, prepared three different region's antibodies against FibH, performed intact FibH electrophoretic band in both SDS-PAGE and immunoblot analysis, and uncovered the molecular nature of the *Nd* mutant. Linkage mapping and functional analysis showed that a deletion of 19 bp in A07 of *FibH*, causing premature translational termination and resulting in a truncated FibH in the *Nd* mutant. Immunostaining observation and immunoblot analysis revealed a fibroin secretion-deficiency in *Nd*-PSG cells. In addition, the genetic hybridization showed a positive correlation between fibroin secretion-deficiency and silk gland atrophy, indicating that secretion-deficient FibH was responsible for the PSG atrophy and naked pupa phenotypes in the *Nd* mutant.

FibH, the major component of silk fibroin, is a high-molecular-weight (350 kDa) structural protein. Excluding the NT and CT, over 90% of its encoding region is a highly repetitive Gly-Ala-rich sequence that contributes to the physical properties of fibroin (Mita et al., 1994; Sanggaard et al., 2014; Zhou et al., 2000). Previous studies of silks revealed that small terminal domains are highly important for the assembly of structure proteins such as collagens or silks (Eisoldt et al., 2012) and that the FibH NT serves as a signal peptide to mediate the assembly of silk in response to decreasing in pH (He et al., 2012; Zhou et al., 2000). In this study, the comparative analysis of FibH structural between *Nd* mutant (NT + repetitive region) and WT/Dazao (NT + repetitive region + CT) showed that the CT might contribute to the efficient secretion of FibH (Fig. 8C). The CT of FibH contains three cysteine residues: the twentieth, fourth, and first cysteine residue from CTD of FibH (Cys-c20, Cys-c4, and Cys-c1, respectively). Among these, Cys-c20 is crucially important for forming a disulfide-link with FibL,

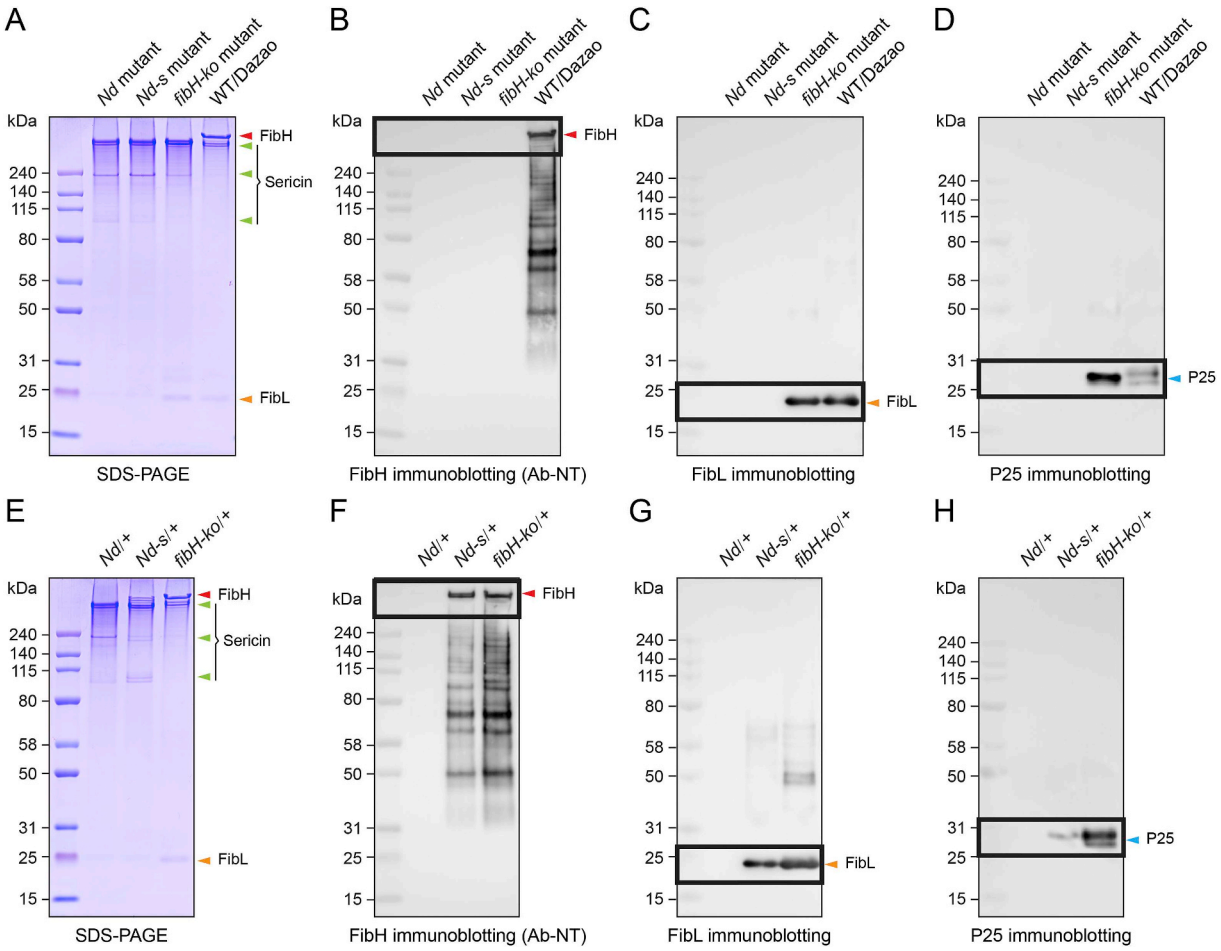

Fig. 7. Immunoblot analysis of three fibroin proteins in cocoon. (A) The SDS-PAGE analysis of total proteins in the cocoon of homozygous mutants. The gel was stained by Coomassie brilliant blue. (B–D) Immunoblot analysis of FibH (B), FibL (C), and P25 (D) in the cocoon of homozygous mutants. (E) The SDS-PAGE analysis of total proteins in the cocoon of heterozygous mutants. The gel was stained by Coomassie brilliant blue. (F–H) Immunoblot analysis of FibH (F), FibL (G), and P25 (H) in the cocoon of heterozygous mutants. The red arrowhead points to the FibH, the orange arrowhead points to the FibL, the blue arrow points to the P25, and the green arrowhead points to the sericin. (For interpretation of the references to color in this figure legend, the reader is referred to the Web version of this article.)

and Cys-c4 and Cys-c1 form an intramolecular disulfide bond (Takei et al., 1987; Tanaka et al., 1999b). Thus, the CT appears to assist the high-molecular-weight/repetitive FibH in folding into the correct protein structure and assembling a functional fibroin unit to promote efficient fibroin secretion.

The repetitive Gly-Ala-rich region of FibH has been studied as a contribution to the mechanical property of the silk fiber (Andersson et al., 2016), but the role of which in fibroin secretion is not entirely clear. In this study, we found that the truncated *Nd*-FibH contained an NT and a repetitive region, with proportions of 4.4% and 95.6%, respectively (Fig. 3D and E, and Fig. S4). Immunostaining observations showed that truncated FibH was not secreted from PSG cells, thus, blocking intracellular transport (Fig. 4B). On the other hand, *fibH-ko-FibH* encoding a protein with 118 aa (only NT of FibH), which can be successfully secreted to PSG lumen due to its low molecular weight (13 kDa) (Ma et al., 2014). As shown in Fig. 7C and D, low molecular weight FibL and P25 (25 kDa and 30 kDa, respectively) are also secreted into the cocoon in *fibH-ko* homozygote, suggesting a normal system of protein secretion in *fibH-ko*-PSG without blocked fibroin in PSG cell. Combined the structure of secretion-deficient *Nd*-FibH (NT and repetitive region) with that of secretion-sufficient *fibH-ko*-FibH (only NT), these findings suggested that the repetitive region played a pathogenic role, and natural fibroin secretion prevented the repetitive region from accumulating in the cell and causing cytotoxicity.

P25/fhx, a glycoprotein, contains three N-linked oligosaccharide chains at Asn69, Asn113, Asn133 (Inoue et al., 2000) and exists either in a 30 kDa (major) and 27 kDa (minor) molecular form (Tanaka et al., 1999a), which has been suggested to have different compositions of oligosaccharide chains (Inoue et al., 2000). The 27 kDa P25/fhx was produced from the 30 kDa form by digestion with the α1,2-mannosidase in Golgi apparatus (Inoue et al., 2004). It is of interest to note that, in immunoblot analysis, the P25 in WT-PSG and WT-cocoon showed two immune bands (27 kDa and 30 kDa), while that of *Nd*-PSG and *fibH-ko*-cocoon showed a single immune band with a molecular weight between the two bands (Figs. 5D and 7D). The common feature between the *Nd* mutant and *fibH-ko* mutant is both of them form a misassembled fibroin unit. Thus, we speculated that a correct fibroin unit was necessary for protein processing of P25, and the single P25 band with a molecular weight between 27 kDa and 30 kDa was undergone different glycosylation in the endoplasmic reticulum and different digestion in Golgi apparatus. The detailed mechanism needs further study.

Fibroin unit (FibH-FibL-P25 complex with a 6:6:1 molar ratio) is the elementary molecular complex for silk fibroin efficient secretion (Inoue et al., 2000, 2004). Since the mutant site was located in the repetitive region of *FibH* (deletion of 19 bp in A07), it was hard to create a similar *Nd* phenotype by designing a specific (low off-target effect) sgRNA and using CRISPR/Cas9 knock-out system in WT silkworm. Since the ORF of WT-*FibH* was almost 16 kb, it was also hard to rescue the *Nd* phenotype by transgenic introducing an intact *FibH* gene in *Nd* mutant silkworm. Therefore genetic analysis was performed to clarify the role of the

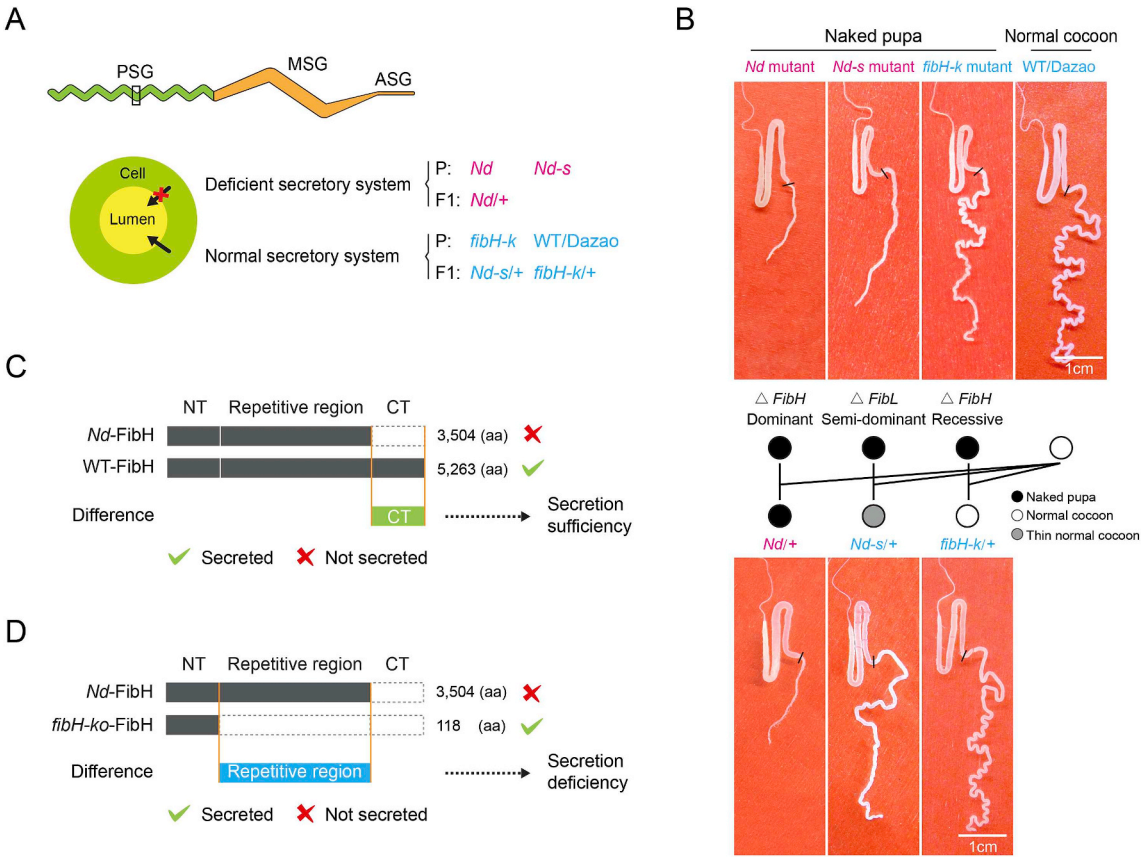

Fig. 8. Positive correlation between fibroin secretion-deficiency and silk gland atrophy. (A) Schematic diagram of the secretory system of PSG in homozygous mutants (*Nd* mutant, *Nd-s* mutant, and *fibH-k* mutant) and heterozygous mutants (*Nd/+* mutant, *Nd-s/+* mutant, and *fibH-k/+* mutant). (B) Silk gland phenotypes of homozygous mutants and heterozygous mutants at the L5D3. (C–D) Substructure comparison of the *Nd*-FibH with WT-FibH (C), and the *Nd*-FibH with *fibH-ko*-FibH (D). Dotted boxes indicate the deleted region of FibH. Green-tick, secreted; Red-cross, not secreted. (For interpretation of the references to color in this figure legend, the reader is referred to the Web version of this article.)

truncated FibH in silk production defects. Molecular weight prediction showed that *Nd*-FibH (Truncated) was 270 kDa, *Nd-s*-FibH (Intact) was 350 kDa, *fibH-ko*-FibH (NT-remaining) was 13 kDa, and WT-FibH (Intact) was 350 kDa. Genetic hybridization experiments analysis showed that the WT-PSG, *fibH-ko*-PSG, *Nd-s/+*−PSG, *fibH-ko/+*−PSG, with a normal system of protein secretion (Fig. 7A–H and 8A), were long and folded (Fig. 8B), however, the *Nd*-PSG, *Nd-s*-PSG, and *Nd/+*−PSG, with a deficient system of protein secretion (Fig. 7A–H and 8A), were short and degenerate (Fig. 8B). By comparing the FibH structure of these three mutations and their PSG phenotype (Fig. 8 B), we learned that secretion-deficient fibroin units invariably contained high-molecular-weight FibH and showed positive correlation with PSG atrophy phenotype. Therefore we inferred that there were two key factors of FibH causing dominant PSG atrophy phenotype: (i) The FibH was of high-molecular-weight/high-repetitive-region; (ii) The FibH was blocked in PSG cell.

It was noteworthy that only the silkworm PSGs carrying the *Nd* mutation were atrophied both in and homozygous and heterozygous individuals (Fig. 8B), a dominant inheritance pattern. The truncated *Nd*-FibH contained only an NT (16 kDa) and a repetitive region (254 kDa), which cannot link to FibL because of lacking CT's Cys. In homozygous *Nd*-PSG, six truncated FibHs, six FibLs, and one P25 failed to assemble a correct fibroin unit; meanwhile in heterozygous *Nd/+*−PSG, three intact FibHs, three truncated FibHs, six FibLs, and one P25 failed to assemble a correct fibroin unit as well. The accumulation of damaged proteins, resulting from mutation/misfolding/aggregation, are pathogenic and can endanger survival under severe stress conditions (Buchberger et al., 2010; Ellgaard and Helenius, 2003). In the present study, the mutant FibH was an aggregation of a single repetitive unit. The incorrect fibroin units with high molecular weight resulted from repetitive region of *Nd*-FibH were secretion-deficient, blocked in PSG cell, and ultimately lead to PSG atrophy both in *Nd* and *Nd/+* silkworm, suggesting that the repetitive region of *Nd*-FibH was pathogenic in a dominant manner.

To date, sericin has been found to be involved in a diverse range of biological activities, such as antagonizing oxidation stress (Dash et al., 2008), anticoagulation activities (Tamada et al., 2004), and promoting cell proliferation (Terada et al., 2005). An increasing number of studies have focused on the utility of sericin in tissue engineering and regenerative medicine (Wang et al., 2014a, 2014b; Xie et al., 2015; Zhang et al., 2017). In this study, we found that fibroin-free sericin could be successfully extracted from the cocoon of *Nd* mutant and its hybrids (Figs. 6B and 7A and E), thus eliminating the macrophage responses that arise from the association of sericin with fibroin (Panilaitis et al., 2003). These findings should enable the development of new medical applications in sericin biomaterials.

Silks play a crucial role in the survival and reproduction of many insects (Sutherland et al., 2010). In the domesticated silkworm *B. mori*, artificial breeding allows for silk-deficient mutants to be well preserved. However, in nature, insects that lose the ability to produce silk as a result of gene mutations, tissue damage, or environmental changes, affect their ability to survive or reproduce. The *FibH* genes of different Lepidoptera are homologous (Fedic et al., 2002). As shown in Fig. S5, the deduced CT sequences of FibH in lepidopteran species *B. mori*, *B. mandarina*, *Y. evonymellus*, *G. mellonella*, and *E. kuehniella* were highly conserved, including conserved positions of all three cysteine residues, and indicating that they may be functional in the same way as in *B. mori*. The results of this study indicate that truncated FibH (deletion of a

partial repetitive domain and entire CT) causes silkworm larvae to lose the ability to produce silk as a dominant genetic character (Figs. 6B and 8B). Therefore, the CT coding sequence of *FibH* has a high potential to be used as a target for gene editing (CT deletion) in the control of lepidopteran pests.

Data availability

The authors confirm that all data underlying the findings are fully available without restriction.

Acknowledgments

We thank Dr. Chun Liu (Southwest University, China) for comments and suggestions on the manuscript, Dr. Sanyuan Ma (Southwest University, China) and Dr. Xiaogang Wang (Southwest University, China) for providing cloning vector, and Prof. Marian R. Goldsmith (University of Rhode Island, USA) for critical reading of the manuscript. This work was supported by grants from the key program of the National Natural Science Foundation of China (31530071), the Chongqing Research Program of Basic Research and Frontier Technology (cstc2017jcyjAX0090), and the Project funded by Chongqing Special Postdoctoral Science Foundation (XmT2018060).

Appendix A. Supplementary data

Supplementary data to this article can be found online at https://doi.org/10.1016/j.ibmb.2019.04.006.

References

Altman, G.H., Diaz, F., Jakuba, C., Calabro, T., Horan, R.L., Chen, J., Lu, H., Richmond, J., Kaplan, D.L., 2003. Silk-based biomaterials. Biomaterials 24, 401–416.
Andersson, M., Johansson, J., Rising, A., 2016. Silk spinning in silkworms and spiders. Int. J. Mol. Sci. 17.
Aramwit, P., Siritientong, T., Srichana, T., 2012. Potential applications of silk sericin, a natural protein from textile industry by-products. Waste Manag. Res.: J. Int. Solid Wastes Publ. Clean. Assoc. ISWA 30, 217–224.
Askarieh, G., Nordling, K., Saenz, A., Casals, C., Rising, A., Johansson, J., Knight, S.D., 2010. Self-assembly of spider silk proteins is controlled by a pH-sensitive relay. Nature 465, 236–238.
Babb, P.L., Lahens, N.F., Correa-Garhwal, S.M., Nicholson, D.N., Kim, E.J., Hogenesch, J.B., Kuntner, M., Higgins, L., Hayashi, C.Y., Agnarsson, I., 2017. The *Nephila clavipes* genome highlights the diversity of spider silk genes and their complex expression. Nat. Genet. 49, 895–903.
Buchberger, A., Bukau, B., Sommer, T., 2010. Protein quality control in the cytosol and the endoplasmic reticulum: brothers in arms. Mol. Cell 40, 238–252.
Craig, C.L., 1997. Evolution of arthropod silks. Annu. Rev. Entomol. 42, 231–267.
Cui, Y., Zhu, Y.A., Lin, Y.J., Chen, L., Feng, Q.L., Wang, W., Xiang, H., 2018. New insight into the mechanism underlying the silk gland biological process by knocking out fibroin heavy chain in the silkworm. BMC Genomics 19.
Dash, R., Acharya, C., Bindu, P.C., Kundu, S.C., 2008. Antioxidant potential of silk protein sericin against hydrogen peroxide-induced oxidative stress in skin fibroblasts. BMB Rep. 41, 236–241.
Eisoldt, L., Thamm, C., Scheibel, T., 2012. Review the role of terminal domains during storage and assembly of spider silk proteins. Biopolymers 97, 355–361.
Ellgaard, L., Helenius, A., 2003. Quality control in the endoplasmic reticulum. Nature reviews. Mol. Cell Biol. 4, 181.
Fedic, R., Zurovec, M., Sehnal, F., 2002. The silk of Lepidoptera. J. Insect Biotechnol. Sericol. 71, 1–15.
Fu, C., Shao, Z., Fritz, V., 2009. Animal silks: their structures, properties and artificial production. Chem. Commun. 6515–6529.
Goldsmith, M.R., Shimada, T., Abe, H., 2005. The genetics and genomics of the silkworm, *Bombyx mori*. Annu. Rev. Entomol. 50, 71–100.
He, Y.X., Zhang, N.N., Li, W.F., Jia, N., Chen, B.Y., Zhou, K., Zhang, J., Chen, Y., Zhou, C.Z., 2012. N-Terminal domain of *Bombyx mori* fibroin mediates the assembly of silk in response to pH decrease. J. Mol. Biol. 418, 197–207.
Hu, W., Liu, C., Cheng, T., Li, W., Wang, N., Xia, Q., 2016. Histomorphometric and transcriptomic features characterize silk glands' development during the molt to intermolt transition process in silkworm. Insect Biochem. Mol. Biol. 76, 95–108.
Inoue, S., Kanda, T., Imamura, M., Quan, G.X., Kojima, K., Tanaka, H., Tomita, M., Hino, R., Yoshizato, K., Mizuno, S., Tamura, T., 2005. A fibroin secretion-deficient silkworm mutant, *Nd-s*^{D}, provides an efficient system for producing recombinant proteins. Insect Biochem. Mol. Biol. 35, 51–59.
Inoue, S., Tanaka, K., Arisaka, F., Kimura, S., Ohtomo, K., Mizuno, S., 2000. Silk fibroin of *Bombyx mori* is secreted, assembling a high molecular mass elementary unit consisting of H-chain, L-chain, and P25, with a 6:6:1 molar ratio. J. Biol. Chem. 275, 40517–40528.
Inoue, S., Tanaka, K., Tanaka, H., Ohtomo, K., Kanda, T., Imamura, M., Quan, G.X., Kojima, K., Yamashita, T., Nakajima, T., Taira, H., Tamura, T., Mizuno, S., 2004. Assembly of the silk fibroin elementary unit in endoplasmic reticulum and a role of L-chain for protection of alpha1,2-mannose residues in N-linked oligosaccharide chains of fibrohexamerin/P25. Eur. J. Biochem. 271, 356–366.
Jin, H.J., Kaplan, D.L., 2003. Mechanism of silk processing in insects and spiders. Nature 424, 1057–1061.
Liu, X., Zhang, K., 2014. Silk fiber—molecular formation mechanism, structure-property relationship and advanced applications. Oligomerization Chem. Biol. Comp. 3.
Ma, S., Shi, R., Wang, X., Liu, Y., Chang, J., Gao, J., Lu, W., Zhang, J., Zhao, P., Xia, Q., 2014. Genome editing of *BmFib-H* gene provides an empty *Bombyx mori* silk gland for a highly efficient bioreactor. Sci. Rep. 4, 6867.
Mita, K., Ichimura, S., James, T.C., 1994. Highly repetitive structure and its organization of the silk fibroin gene. J. Mol. Evol. 38, 583–592.
Mori, K., Tanaka, K., Kikuchi, Y., Waga, M., Waga, S., Mizuno, S., 1995. Production of a chimeric fibroin light-chain polypeptide in a fibroin secretion-deficient naked pupa mutant of the silkworm *Bombyx mori*. J. Mol. Biol. 251, 217–228.
Nakano, Y., 1951. Physiological, anatomical and genetical studies on the “Naked” silkworm pupa. J. Seric. Sci. Jpn. 20, 232–248.
Oberprieler, R.G., Marvaldi, A.E., Anderson, R.S., 2007. Weevils, weevils, weevils everywhere. Zootaxa 1668, 491–520.
Okada, S., Weisman, S., Trueman, H.E., Mudie, S.T., Haritos, V.S., Sutherland, T.D., 2008. An Australian webspinner species makes the finest known insect silk fibers. Int. J. Biol. Macromol. 43, 271–275.
Omenetto, F.G., Kaplan, D.L., 2010. New opportunities for an ancient material. Science 329, 528–531.
Panilaitis, B., Altman, G.H., Chen, J., Jin, H.J., Karageorgiou, V., Kaplan, D.L., 2003. Macrophage responses to silk. Biomaterials 24, 3079–3085.
Rudall, K., 1962. Silk and other cocoon proteins. Comp. Biochem. 4, 397–433.
Sanggaard, K.W., Bechsgaard, J.S., Fang, X., Duan, J., Dyrlund, T.F., Gupta, V., Jiang, X., Cheng, L., Fan, D., Feng, Y., Han, L., Huang, Z., Wu, Z., Liao, L., Settepani, V., Thogersen, I.B., Vanthournout, B., Wang, T., Zhu, Y., Funch, P., Enghild, J.J., Schauser, L., Andersen, S.U., Villesen, P., Schierup, M.H., Bilde, T., Wang, J., 2014. Spider genomes provide insight into composition and evolution of venom and silk. Nat. Commun. 5, 3765.
Sattler, W., 1967. Über die Lebensweise, insbesondere das bauverhalten, neotropischer eintagsfliegen larven (Ephemeroptera: Polymitarcidae) Beitr. Neotrop. Fauna 5, 89–110.
Shao, Z., Vollrath, F., 2002. Surprising strength of silkworm silk. Nature 418, 741.
Sturm, H., 1992. Mating-behavior and sexual dimorphism in *Promesomachilis hispanica* Silvestri, 1923 (Machilidae, Archaeognatha, Insecta). Zool. Anz. 228, 60–73.
Sutherland, T.D., Weisman, S., Trueman, H.E., Sriskantha, A., Trueman, J.W., Haritos, V.S., 2007. Conservation of essential design features in coiled coil silks. Mol. Biol. Evol. 24, 2424–2432.
Sutherland, T.D., Young, J.H., Weisman, S., Hayashi, C.Y., Merritt, D.J., 2010. Insect silk: one name, many materials. Annu. Rev. Entomol. 55, 171–188.
Takei, F., Kikuchi, Y., Kikuchi, A., Mizuno, S., Shimura, K., 1987. Further evidence for importance of the subunit combination of silk fibroin in its efficient secretion from the posterior silk gland cells. J. Cell Biol. 105, 175–180.
Tamada, Y., Sano, M., Niwa, K., Imai, T., Yoshino, G., 2004. Sulfation of silk sericin and anticoagulant activity of sulfated sericin. J. Biomater. Sci. Polym. Ed. 15, 971–980.
Tanaka, K., Inoue, S., Mizuno, S., 1999a. Hydrophobic interaction of P25, containing Asn-linked oligosaccharide chains, with the H-L complex of silk fibroin produced by *Bombyx mori*. Insect Biochem. Mol. Biol. 29, 269–276.
Tanaka, K., Kajiyama, N., Ishikura, K., Waga, S., Kikuchi, A., Ohtomo, K., Takagi, T., Mizuno, S., 1999b. Determination of the site of disulfide linkage between heavy and light chains of silk fibroin produced by *Bombyx mori*. Biochim. Biophys. Acta 1432, 92–103.
Terada, S., Sasaki, M., Yanagihara, K., Yamada, H., 2005. Preparation of silk protein sericin as mitogenic factor for better mammalian cell culture. J. Biosci. Bioeng. 100, 667–671.
Teramoto, H., Kojima, K., 2014. Production of *Bombyx mori* silk fibroin incorporated with unnatural amino acids. Biomacromolecules 15, 2682–2690.
Vollrath, F., 1999. Biology of spider silk. Int. J. Biol. Macromol. 24, 81–88.
Wang, F., Xu, H., Wang, Y., Wang, R., Yuan, L., Ding, H., Song, C., Ma, S., Peng, Z., Peng, Z., Zhao, P., Xia, Q., 2014a. Advanced silk material spun by a transgenic silkworm promotes cell proliferation for biomedical application. Acta Biomater. 10, 4947–4955.
Wang, J., Xia, Q., He, X., Dai, M., Ruan, J., Chen, J., Yu, G., Yuan, H., Hu, Y., Li, R., Feng, T., Ye, C., Lu, C., Wang, J., Li, S., Wong, G.K., Yang, H., Wang, J., Xiang, Z., Zhou, Z., Yu, J., 2005. SilkDB: a knowledgebase for silkworm biology and genomics. Nucleic Acids Res. 33, D399–D402.
Wang, Y.J., Nakagaki, M., 2014. Editing of the heavy chain gene of *Bombyx mori* using transcription activator like effector nucleases. Biochem. Biophys. Res. Commun. 450, 184–188.
Wang, Z., Zhang, Y., Zhang, J., Huang, L., Liu, J., Li, Y., Zhang, G., Kundu, S.C., Wang, L., 2014b. Exploring natural silk protein sericin for regenerative medicine: an injectable, photoluminescent, cell-adhesive 3D hydrogel. Sci. Rep. 4, 7064.
Xia, Q., Li, S., Feng, Q., 2014. Advances in silkworm studies accelerated by the genome sequencing of *Bombyx mori*. Annu. Rev. Entomol. 59, 513–536.
Xia, Q., Zhou, Z., Lu, C., Cheng, D., Dai, F., Li, B., Zhao, P., Zha, X., Cheng, T., Chai, C., Pan, G., Xu, J., Liu, C., Lin, Y., Qian, J., Hou, Y., Wu, Z., Li, G., Pan, M., Li, C., Shen, Y., Lan, X., Yuan, L., Li, T., Xu, H., Yang, G., Wan, Y., Zhu, Y., Yu, M., Shen, W., Wu, D., Xiang, Z., Yu, J., Wang, J., Li, R., Shi, J., Li, H., Li, G., Su, J., Wang, X., Li, G.,

Zhang, Z., Wu, Q., Li, J., Zhang, Q., Wei, N., Xu, J., Sun, H., Dong, L., Liu, D., Zhao, S., Zhao, X., Meng, Q., Lan, F., Huang, X., Li, Y., Fang, L., Li, C., Li, D., Sun, Y., Zhang, Z., Yang, Z., Huang, Y., Xi, Y., Qi, Q., He, D., Huang, H., Zhang, X., Wang, Z., Li, W., Cao, Y., Yu, Y., Yu, H., Li, J., Ye, J., Chen, H., Zhou, Y., Liu, B., Wang, J., Ye, J., Ji, H., Li, S., Ni, P., Zhang, J., Zhang, Y., Zheng, H., Mao, B., Wang, W., Ye, C., Li, S., Wang, J., Wong, G.K., Yang, H., Biology Analysis, G., 2004. A draft sequence for the genome of the domesticated silkworm (*Bombyx mori*). Science 306, 1937–1940.

Xie, H., Yang, W., Chen, J., Zhang, J., Lu, X., Zhao, X., Huang, K., Li, H., Chang, P., Wang, Z., Wang, L., 2015. A silk sericin/silicone nerve guidance conduit promotes regeneration of a transected sciatic nerve. Adv. Healthc. Mater. 4, 2195–2205.

Yamamoto, K., Nohata, J., Kadono-Okuda, K., Narukawa, J., Sasanuma, M., Sasanuma, S., Minami, H., Shimomura, M., Suetsugu, Y., Banno, Y., Osoegawa, K., de Jong, P.J., Goldsmith, M.R., Mita, K., 2008. A BAC-based integrated linkage map of the silkworm *Bombyx mori*. Genome Biol. 9, R21.

Yonemura, N., Sehnal, F., 2006. The design of silk fiber composition in moths has been conserved for more than 150 million years. J. Mol. Evol. 63, 42–53.

Yonemura, N., Sehnal, F., Mita, K., Tamura, T., 2006. Protein composition of silk filaments spun under water by caddisfly larvae. Biomacromolecules 7, 3370–3378.

Zhang, L., Yang, W., Tao, K., Song, Y., Xie, H., Wang, J., Li, X., Shuai, X., Gao, J., Chang, P., Wang, G., Wang, Z., Wang, L., 2017. Sustained local release of NGF from a chitosan-sericin composite scaffold for treating chronic nerve compression. ACS Appl. Mater. Interfaces 9, 3432–3444.

Zhou, C.Z., Confalonieri, F., Medina, N., Zivanovic, Y., Esnault, C., Yang, T., Jacquet, M., Janin, J., Duguet, M., Perasso, R., Li, Z.G., 2000. Fine organization of *Bombyx mori* fibroin heavy chain gene. Nucleic Acids Res. 28, 2413–2419.